VISCOELASTIC RESPONSE OF THE HUMAN BRAIN TO SAGITTAL AND LATERAL ROTATIONAL ACCELERATION BY FINITE ELEMENT ANALYSIS

Chun Zhou, Tawfik B. Khalil, Albert I. King

Bioengineering Center
Wayne State University
Detroit, Michigan, USA

ABSTRACT

A new three-dimensional human head finite element model, the WSU Brain Injury Model, representing a 50th percentile male human head, was used to study brain response to rotational impacts. An angular acceleration pulse taken from Abel's monkey test data (1978) was scaled to study human brain response. The scaling method used maintained approximately equal shear strain level in the brain and equal displacement of the head. Viscoelastic responses of the brain to impulsive sagittal and lateral rotational accelerations were obtained. Differences in brain response between sagittal and lateral rotational impact were found. The influence of the brain material properties on model response was investigated.

BRAIN INJURY is still a major unsolved problem in many respects. Finite element modeling of head impact proved to be a useful method of investigating the mechanical response of the head, establishing brain injury mechanisms and providing analytical stress/strain measures to evaluate corresponding injury criteria, particularly when used in conjunction with appropriate experimental studies. Recent brain injury research at the Bioengineering Center of Wayne State University has focused on the biomechanics of brain injury by developing a comprehensive 50th percentile male human head model which, when fully validated, is expected to be capable of predicting human head impact response and delineating impact injury mechanisms. The WSU Brain Injury Model developed by Zhou et al (1995) is a continuation of the modeling efforts of the two-dimensional porcine brain models by Zhou et al (1994) and the three-dimensional human head model by Ruan et al (1994). All of these models were subjected to qualitative or partially quantitative validations against experimental data.

Shear deformation of the brain due to head rotation has long been postulated as a major cause of brain injury because of the very low shear stiffness of brain

tissue (Holbourn, 1943). Animals, physical models and finite element models have been used to investigate brain response due to rotational impacts. But three-dimensional finite element simulations of rotational impacts are rare and little information on the distribution of shear stress/strain of the human brain due to rotational impact is available. The WSU Brain Injury Model was exercised to investigate elastic responses to an impulsive sagittal plane rotation (Zhou et al, 1995), producing useful insights into the problem. In this study, the model was exercised to investigate viscoelastic responses to sagittal and/or lateral rotational impacts. An angular acceleration pulse taken from Abel's monkey test data (1978) was scaled to provide input for the human brain.

MODEL DESCRIPTIONS AND METHODS

NEW FEATURES OF THE WSU BRAIN INJURY MODEL The WSU Brain Injury Model, shown in Figure 1, consisted of the scalp, skull, dura, falx, tentorium, pia, CSF, venous sinuses, ventricles, cerebrum (gray and white matter), cerebellum, brain stem and bridging veins. The geometry of the head model was based on an atlas by McGrath and Mills(1984), and on brain sections prepared in our laboratory. The locations of the bridging veins were based on Oka et al (1985). The overall geometry of the model represented a 50th percentile male human head. The head consisted of 17656 nodes and 22995 elements. Its total mass was 4.37 kg with the brain being 1.41 kg. Details of the model can be found in Zhou (1995).

One of the distinctive features of the model is the differentiation of the gray and white matter. The irregular boundaries between the gray and white matter were simulated in the model, but were greatly simplified. Different material properties were used for the gray and white matter. The inhomogeneous nature of the brain can be better simulated with these geometrical and constitutive descriptions.

Another new feature is the inclusion of the ventricles in the model. The corners of the ventricles are common sites of DAI (Diffuse Axonal Injury). Without ventricular representation in the model, stress concentrations around ventricles could not be produced in our previous study (Zhou et al, 1994).

Figure 2 shows a third new feature - modeling of ten pairs of parasagittal bridging veins with string elements. It was the first attempt to simulate bridging veins in a human head finite element model. With these bridging veins, their impact response can be analyzed and the mechanisms of subdural hematomas can be investigated by computer modeling.

VISCOELASTIC MATERIAL PROPERTIES OF THE BRAIN Material properties of the brain tissues are difficult to measure. There is no effective way to measure material properties of the brain tissues which have thus far been treated as homogeneous gel-like materials. It was reported (McElhaney et al, 1969; Estes and McElhaney, 1970) that human and monkey brains are substantially incompressible with a strain-rate independent bulk modulus of 2.07 GPa, very close to that of water. The dynamic complex shear modulus of a human autopsy brain has been measured by vibration tests. Some results from different tests are summarized below:
G_1 = 0.60 - 1.10 kPa, G_2 = 0.35 - 0.60 kPa, G_2/G_1 = 0.40-0.55, at 10 Hz,

(Fallenstein et al, 1970),
G_1 = 0.43 - 0.95 kPa, G_2 = 0.35 - 0.60 kPa, G_2/G_1 = 0.72, at 9-10 Hz,
(McElhaney et al,1973),
G_1 = 0.83 - 138.00 kPa, G_2 = 0.34 - 82.70 Kpa, at 2-400 Hz,
(Shuck et al, 1970),
G_1 = 7.60 - 33.90 Kpa, G_2 = 2.76 - 81.60 Kpa, at 5-350 Hz,
(Shuck et al, 1972),
where G_1 stands for storage shear modulus and G_2 for loss shear modulus. The dynamic complex tensile modulus of human brain tissue from vibration tests by Galford and McElhaney (1970) are: storage modulus E_1 = 66.7 Kpa and loss modulus E_2 = 26.2 Kpa at 34 Hz.

The most recent effort was made by Arbogast et al (1995). Vibration tests were performed over a range of 20 - 100 Hz to determine the complex shear modulus of newborn porcine brain stems. An equivalent shear modulus of 2.3 - 2.9 kPa was proposed.

The considerable variation in the test data shows that the material properties of the brain have not been finally established. However, there is definite evidence that the brain does exhibit viscoelasticity and brain modelers have been trying to make their best estimates of an appropriate shear relaxation function. Some material properties used in linearly viscoelastic head models are summarized in Table 1.

Table 1 Material properties of the brain used in linear viscoelastic models.

Reference	G_0 (kPa)	G_∞ (kPa)	β (s^{-1})	K (MPa)
Khalil & Viano (1977)	49.0	16.2	145	
Galbraith & Tong (1988) (gel)	11.02	5.512	200	
Cheng et al (1990) (gel)	35-70	7.51	50-300	
Lee (1990) (gel)	26.9-110	2.87-	50	1.25-5.44
DiMasi et al (1991)	34.474	17.23	100	68.948
Ruan (1994)	528	168	35	127.9

G_∞ - long term shear modulus, G_0 - short term shear modulus, β - decay factor, K - bulk modulus.

In this study, we used Shuck's data (1972) to deduce the shear modulus. The empirical interconversion equation by Christensen (1982)

$$G(t) = G'(\omega)\big|_{\omega = 2/\pi t}$$

was used to convert test data in the frequency domain to the time domain. Shear modulus parameters were determined from a logarithmic plot:

G_0 = 41 kPa, G_∞ = 7.6 kPa, β = 700 s^{-1} for white matter,
G_0 = 34 kPa, G_∞ = 6.3 kPa, β = 700 s^{-1} for gray matter.

where G_0 is the short term shear modulus, G_∞ is the long term shear modulus and β is decay factor. We assumed that the white and gray matter had the same decay factor but the shear modulus of the white matter was higher than that of the gray

matter. The only justification for this assumption is that white matter should be stronger and tougher because it is composed of axonal fibers and gray matter is composed of nerve cell bodies. The bulk modulus K = 2.19 GPa was used for both materials. In Figure 3, Curve A is the exponential relaxation function while Curve B is based on our curve fitting for white matter with $\beta = 700\ s^{-1}$. Curve C, used as the upper bound of the relaxation function, is for $\beta = 70\ s^{-1}$, Curve D is taken from Khalil & Viano (1977), and Curve E is from DiMasi et al (1991).

The above deduced viscoelastic moduli were used as baseline for both sagittal and lateral rotational impacts. In addition, five more runs were performed for sagittal rotation with different brain material parameters to study the influence of brain material properties on model response. Changing β to $70\ s^{-1}$ from the baseline was the Case B-70 to get results for the upper bound. Case SG50 assumed a 50% higher shear modulus for the white matter than that for the gray matter with $\beta = 700\ s^{-1}$. Case SG50-B70 was for the upper bound for Case SG50 with $\beta = 70\ s^{-1}$. Case E-MAX was the elastic analysis assuming the shear modulus of G_0 used for the baseline. Case E-MINwas the elastic analysis assuming the shear modulus of G_∞ used for the baseline. The material properties used in this study are listed in Table 2.

Table 2. Material properties of the brain used for parametric study

	G_0 (kPa)		G_∞ (kPa)		β (s^{-1})
Base	41	34	7.6	6.3	700
B-70	41	34	7.6	6.3	70
SG50	51	34	9.5	6.3	700
SG50-B70	51	34	9.5	6.3	70
E-MAX	G = 41	G = 34			
E-MIN			G=7.6	G=6.3	
	white	gray	white	gray	

SCALING OF TEST DATA FOR MODEL INPUT To extrapolate impact test results obtained from animals to human beings, a scaling relationship must be established. Ommaya et al (1967) applied Holbourn's scaling law

$$\ddot{\theta}_1 = \ddot{\theta}_2 \left(\frac{M_2}{M_1}\right)^{2/3} \qquad (1)$$

where $\ddot{\theta}$ = angular acceleration, M = brain mass, to predict concussion threshold for man from monkey test data. Margulies et al (1985) also used this scaling law in their physical model tests. This kind of scaling is not complete. For dynamic problems, scaling of time should also be considered.

If the brain is idealized as a sphere with a radius R, it can be shown that to have same stress level in two different sizes of the brain, the scaling for translational

acceleration is

$$\frac{a_1}{a_2} = \frac{R_2}{R_1} = \left(\frac{M_2}{M_1}\right)^{1/3} \quad (2)$$

and that for rotational acceleration is

$$\frac{\ddot{\theta}_1}{\ddot{\theta}_2} = \left(\frac{R_2}{R_1}\right)^2 = \left(\frac{M_2}{M_1}\right)^{2/3} \quad (3)$$

Time scaling is established by the requirement to have same translation

$$\frac{t_1}{t_2} = \left(\frac{R_1}{R_2}\right)^{1/2} = \left(\frac{M_1}{M_2}\right)^{1/6} \quad (4)$$

and same rotation

$$\frac{t_1}{t_2} = \frac{R_1}{R_2} = \left(\frac{M_1}{M_2}\right)^{1/3} \quad (5)$$

In this study, the scaling was done according to above equations, assuming that R = 68 mm for the human brain, R = 26 mm for the rhesus monkey brain. The angular acceleration pulse was taken from Abel's tests (1978). Figure 4 shows the original test data and the scaled angular acceleration for model input. The input angular acceleration impulse is expanded as shown in Figure 5 for clarity. A peak angular acceleration of 7,030 rad/s ^{2} occurred at about 4 ms and the peak angular deceleration of 9,192 rad/s ^{2} was reached at about 32 ms. These values are well within the normal range of angular acceleration magnitudes sustained by the human head in field accidents. The head was forced to rotate about a lateral +Y-axis (right to left) for sagittal plane rotations, and about an anterior-posterior +X-axis for lateral rotations. The maximum angular displacement was about 60 deg.

RESULTS AND DISCUSSIONS

Figure 6 shows the kinetic energies imparted to the brain during a rotational impact. The kinetic energy due to sagittal rotation (Curve A) is virtually the same as that due to lateral rotation (Curve B). This was achieved by adjusting the center of rotation of the model. The resulting strain energy (Curve D, 5.17 J) due to sagittal rotation about a transverse axis (right to left) is higher than that (Curve C, 4.30 J) due to lateral rotation about a longitudinal axis (in the A-P direction). This is due to that fact that the head moment of inertia about the longitudinal axis is lower than that about the transverse axis. The skull has less resistance to prevent the brain from lateral rotation. Therefore, the same loading will result in a larger deformation of the brain in lateral rotation than that in sagittal rotation. This is consistent with experimental observations by Gennarelli et al (1987) that lateral head impacts

produced more severe DAI in the monkeys.

Figures 7 and 8 show the shear stresses and strains developed in the genu of the corpus callosum. Sagittal rotations produced a higher shear in the genu. The peak shear stress was 8.81 kPa for sagittal rotation (Curve A, SG-BASE), but only 1.97 kPa for lateral rotation (Curve B, LT-BASE). The corresponding peak shear strain was 0.289 for sagittal rotation (Curve A, SG-BASE) and 0.069 for lateral rotation (Curve B, LT-BASE). Note that the stress time histories are not of the same shape of as those for strain because of viscoelasticity. The first peak shear stress occurred at about 4 ms for Curve A in Figure 7 while the first peak shear strain occurred at about 7 - 8 ms for Curve A in Figure 8.

When $\beta = 70\ s^{-1}$ (Curve C, B70), the peak shear stress increased to 18.5 kPa and the corresponding peak shear strain decreased to 0.256. Similar changes were seen from Case SG50 (Curve C) to Case SG50-B70 (Curve D), the peak shear stress increased from 10.6 kPa to 21.8 kPa and the corresponding peak shear strain decreased from 0.281 to 0.242. Therefore, the decay factor has a great influence over the magnitude of the peak shear stress, and less influence over the magnitude of the peak shear strain. Note that changes in decay factor do not change shear deformation pattern.

When the shear modulus for the white matter was changed from about 20% higher than that of the gray matter to 50% higher, the peak shear stress increased from 8.81 kPa (Curve A, SG-BASE) to 10.6 kPa (Curve D, SG50), and the corresponding peak shear strain decreased from 0.289 to 0.281. The difference between these two cases was not significant.

The results of the elastic analysis Case E-MAX, using the shear modulus of G_0 for the baseline case, formed the upper bound for the peak shear stresses (Curve F, E-MAX, Figure 7) and lower bound for the peak shear strains (Curve F, E-MAX, Figure 8). The results of Case E-MIN, using the shear modulus of G_∞ for the baseline case, formed the lower bound for the peak shear stresses (Curve G, E-MIN, Figure 7) and upper bound for the peak shear strains (Curve G, E-MIN, Figure 8). The responses of the viscoelastic cases were basically located within the corridor formed by Case E-MAX and Case E-MIN. Curve E for Case SG50-B70 was not covered by the corridor because the shear modulus of the brain for Case SG50-B70 was beyond the range of the elastic shear modulus. The results of the elastic and viscoelastic analyses showed a similar trend. However, the peak time for viscoelastic analysis was ahead of that for elastic analysis. If we are only interested in a limit analysis, the elastic analysis can provide a reasonable estimate of the shear response of the brain if the range of the shear moduli for the brain are known.

Shown in Figure 9 are the axial strains of the central bridging vein which sustained highest stretch in both sagittal and lateral rotations. The axial strains of the bridging veins due to lateral rotation were much lower. In sagittal rotation it experienced a strain of 0.383 (Curve A, SG-BASE), but in lateral rotation the strain was as low as 0.081 (Curve B, LT-BASE16). So the risk of subdural hematoma in a sagittal rotational impact can be 4 times as large as that in a lateral rotational impact.

The material properties of the brain also showed influence over the stretch of

the parasagittal bridging veins. When $\beta = 70\ s^{-1}$, the axial strain decreased from 0.383 (Curve A, SG-BASE) to 0.33 (Curve D, B70), and from 0.376 (Curve E, SG50) to 0.32 (Curve F, SG50-B70). Difference between Case SG-BASE and Case SG50 was not significant. The elastic cases also formed upper bound of 0.43 (Curve H, E-MIN) and lower bound of 0.32 (Curve G, E-MAX). The results showed that when higher shear moduli were used for the brain, the axial strains of the bridging veins decreased.

Shown in Figure 10 are the axial strains of the parasagittal bridging veins due to sagittal rotation (Case BASE). Except for the backward-facing bridging veins of the frontopolar (A), the anterior frontal (B) and the middle frontal (C) which were in tension during the deceleration phase, the forward-facing bridging veins from the posterior frontal (D) to the occipital (J) were under higher tensile strains during the acceleration phase. These results indicated that the bridging veins would rupture during the acceleration phase. In particular, the posterior frontal to the occipital veins would be at a higher risk of rupture. These results are consistent with the findings in the animal tests by Abel et al (1978) in which subdural hematomas originating in the parasagittal bridging veins were found in 16 out of the 40 experiments. However, these results also tend to support Lee and Haut's (1989) arguments that subdural hematoma in the animal tests by Gennarelli and Thibault (1982) could have occurred during the accelerating phase.

Shear stress contours in a parasagittal section at 32 ms are shown in Figure 11 (sagittal rotation) and Figure 12 (lateral rotation). The maximum principal shear stress due to lateral rotation was 5 kPa, higher than the 3.5 kPa due to sagittal rotation. High shear stresses occurring in the midbrain tegmentum and the thalamus predicted a higher risk of DAI in these area for both cases.

Shear stress contours in a coronal section through the level of the anterior commissure at 32 ms are shown in Figure 13 (sagittal rotation) and Figure 14 (lateral rotation). High shear stresses at the inferior horns of the lateral ventricles can be observed for both cases. Shear stresses in the corpus callosum were more prominent in sagittal rotation while shear stresses near the upper cortexes were more prominent in lateral rotation. Shear stress concentrations at the corpus callosum can be observed for both cases. Large shear deformations in the coronal plane of the brain can be observed in lateral rotation. These shear stress contours reveal high shear stresses in the midbrain tegmentum and hippocampus (Figure 15 for sagittal rotation, Figure 16 for lateral rotation).

CONCLUSIONS

1. Viscoelastic responses of the brain to rotational impacts have been investigated using the WSU Brain Injury Model. Simulation results were qualitatively consistent with clinically observed injuries.

2. A new scaling method based on the equal stress and displacement requirement was introduced. It accounted for both magnitude and duration of impact. Hopefully, it can be validated to predict human head injury tolerance from animal test data in the future.

3. The same loading would result in higher shear stresses in the brain in lateral rotation than in sagittal rotation. However, the maximum shear stress in the genu is still higher in sagittal rotation.

4. The stretch of the bridging veins in a sagittal plane impact is much higher than in a lateral plane impact. Acceleration of the head in forward flexion (occipital impact) produces the highest tensile strains in most bridging veins.

5. The results of the elastic and viscoelastic analyses showed a similar trend. The elastic analysis can provide a reasonable estimate of the shear response of the brain if the range of the shear moduli for the brain are known.

6. When higher shear moduli were used for the brain, the axial strains of the bridging veins decreased.

ACKNOWLEDGEMENTS

This study was supported in part by the National Center for Injury Prevention and Control of the CDC, Grant No. R94/CCR503534-06. Its contents are solely the responsibility of the authors and do not necessarily represent the official views of the National Center for Injury Prevention and Control of the CDC.

REFERENCES

Abel, J. M., Gennarelli, T. A., Segawa, H. (1978). Incidence and severity of cerebral concussion in the rhesus monkey following sagittal plane angular acceleration. *Proc. 22nd Stapp Car Crash Conf.*, SAE Paper No. 780886.

Arbogast, K. B., Meaney, D. F., Thibault, L. E. (1995). Biomechanical characterization of the constitutive relationship for the brainstem. *Proc. 39th Stapp Car Crash Conference* , SAE Paper No. 952716.

Cheng, L. Y., Rifai, S., Khatua, T., Piziali, R. L. (1990). Finite element analysis of diffuse axonal injury. *Vehicle Crashworthiness and Occupant Protection in Frontal Collisions,* SAE Paper No. 900547.

Christensen, R. M. (1982). Theory of viscoelasticity. 2nd ed., Academic Press, New York.

Dimasi, F., Marcus, J., Eppinger, R. (1991). 3-D anatomic brain model for relating cortical strains to automobile crash loading. *Proc. 13th int. Tech. Conf. on Experimental Safety Vehicles* , Paper No. 91-S8-O-11.

Estes, M. S. and McElhaney, J. H. (1970). Response of brain tissue to compressive loading. ASME Paper No. 70-BHF-13.

Fallenstein, G. T., Hulce, V. D. and Melvin, J. W. (1970). Dynamic mechanical properties of human brain tissue. *J Biomech.*, 2:217-226.

Galbraith, C. G. and Tong, P. (1988). Boundary conditions in head injury finite element modeling. *16th Annu. Int. Workshop on Human Subjects for Biomechanical Research,* pp 179-193.

Galford, J. E., McElhaney, J. H. (1970). A viscoelastic study of scalp, brain, and dura. *J Biomech.*, 3:211-221.

Gennarelli, T. A. and Thibault, L. E. (1982). Biomechanics of acute subdural

hematoma. *J Trauma,* 22:680-686.

Gennarelli, T. A., Thibault, L. E., Tomei, G., Wiser, R., Graham, D., Adams, J. (1987). Directional dependence of axonal brain injury due to centroidal and non-centroidal acceleration. *Proc. 31st Stapp Car Crash Conf.*, SAE Paper No. 872197

Holbourn, A. H. (1943). Mechanics of head injury. *The Lancet,* 2:438-441.

Khalil, T. B. and Viano, D. C. (1977). Impact response of a viscoelastic head model. *General Motors Research Publication* GMR-2380.

Lee, E.-S. (1990). A large-strain, transient-dynamic analysis of head injury problems by finite element method. Ph.D. Dissertation, Georgia Institute of Technology.

Lee, M.-C. and Haut, R.C. (1989). Insensitivity of tensile failure properties of human bridging veins to strain rate: implications in biomechanics of subdural hematoma. *J. Biomech* ., 22:537-542.

McElhaney, J. H., Stalnaker, R. L., Estes, M. S. and Rose, L. S. (1969). Dynamic mechanical properties of scalp and brain. *Proc. 6th Annual Rocky Mountain Bioengineering Symp.* , Laramie, pp 67-73.

Gennarelli, R.A. and Thibault, L.E. (1982). Biomechanics of acute subdural hematoma. *J. Trauma,* 22:680-686.

McElhaney, J. H., Melvin, J. W., Roberts, V. L. and Portnoy, H. D. (1973). Dynamic characteristics if the tissues of the head. *Perspectives in Biomedical Engineering,* Kenedi, R.M., ed., MacMillan Press, London, pp 215-222.

McGrath, P. and Mills, P. (1984). *Atlas of sectional anatomy: head, neck and trunk.* Krage, Basel, Switzland; New York.

Oka, K. et al (1985). Microsurgical anatomy of the superficial veins of the cerebrum. *Neurosurg.,* 17:711-748.

Ommaya, A. K., Yarnell, P., Hirsch, A. E., Harris, E. H. (1967). Scaling of experimental data on cerebral concussion in sub-human primates to concussion threshold for man. *Proc. 11th Stapp Car Crash Conference* , SAE Paper No. 670906.

Ruan, J. S. (1994). Impact biomechanics of head injury by mathematical modeling. Ph.D. Dissertation, Wayne State University.

Ruan, J. S., Khalil, T. B., King, A. I. (1994). Dynamic response of the human head to impact by three-dimensional finite element analysis. ASME *J. Biomech. Engrg.,* 116:44-50.

Shuck, L. Z., Haynes, R. R. and Fogle, J. L. (1970). Determination of viscoelastic properties of human brain tissue. ASME Paper No. 70-BHF-12.

Shuck, L. Z. and Advani, S. H. (1972). Rheological response of human brain tissue in shear. *J Basic Eng.* , pp 905-911.

Zhou, C., Khalil, T. B., and King, A. I. (1994). Shear stress distribution in the porcine brain due to rotational impact. *Proc. 38th Stapp Car Crash Conference* , SAE Paper No. 942214.

Zhou, C., Khalil, T. B., and King, A. I. (1995). A new model comparing impact responses of the homogeneous and inhomogeneous human brain. *Proc. 39th Stapp Car Crash Conference* , SAE Paper No. 952714.

Zhou, C. (1995). Finite element modeling of impact response of an inhomogeneous brain. Ph.D. Dissertation, Wayne State University.

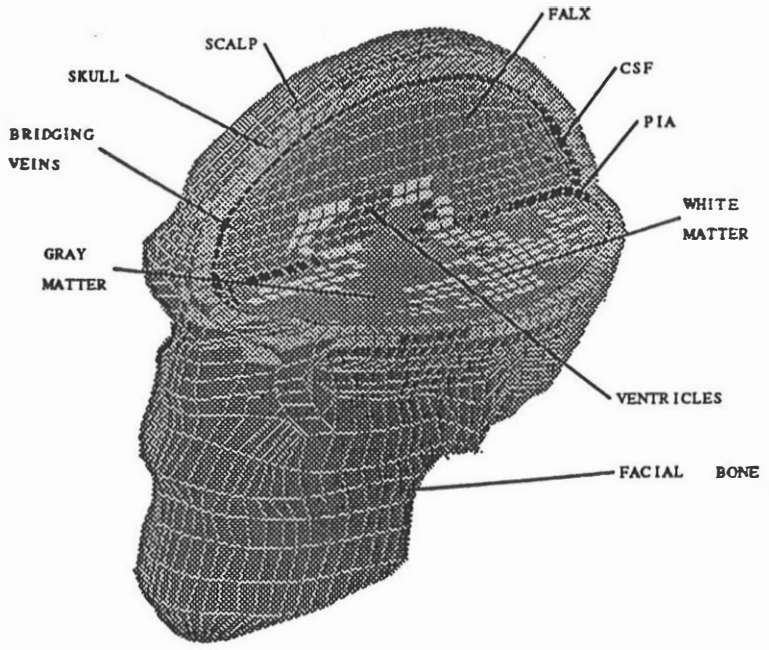

Fig. 1 The WSU Brain Injury Model: overview.

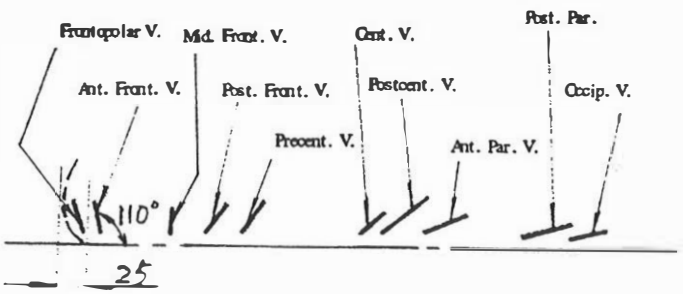

(a) Top view

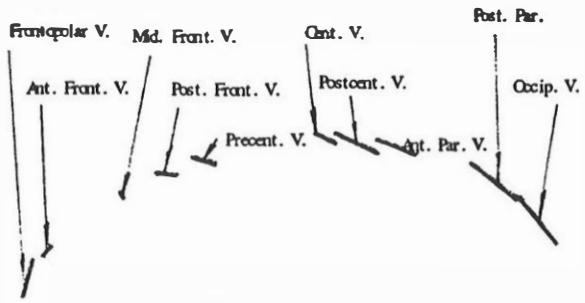

(b) Lateral view

Fig. 2 The parasagittal bridging veins.

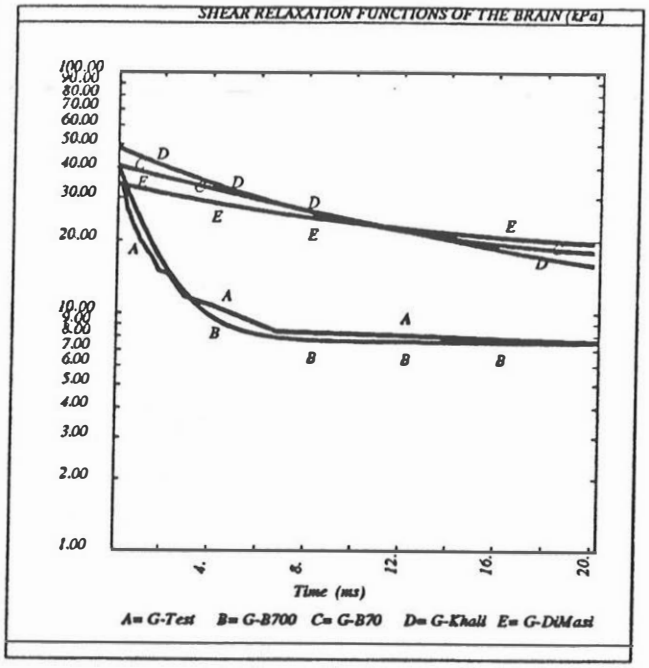

Fig. 3 Shear relaxation functions for the brain.

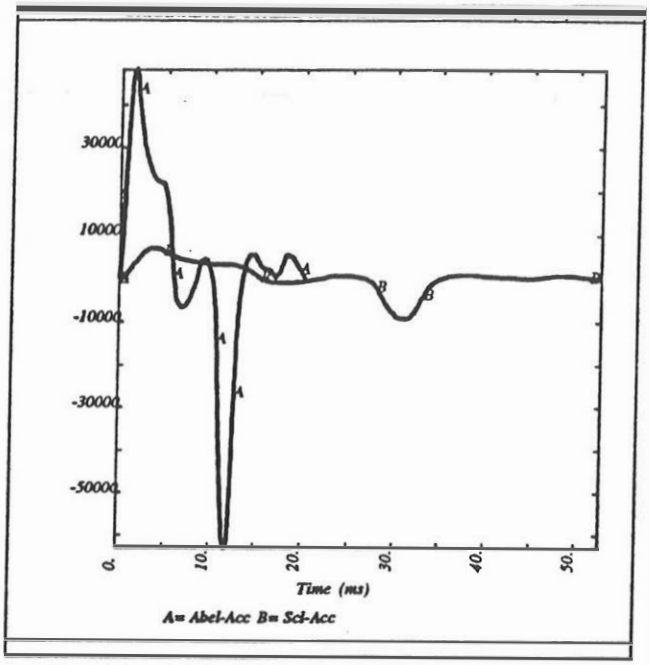

Fig. 4 Original and scaled angular acceleration impulse.

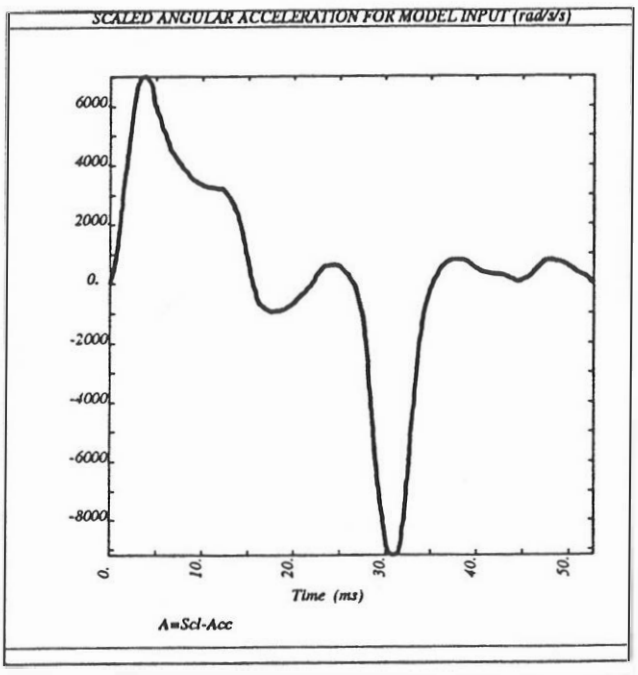

Fig. 5 Angular acceleration impulse for model input.

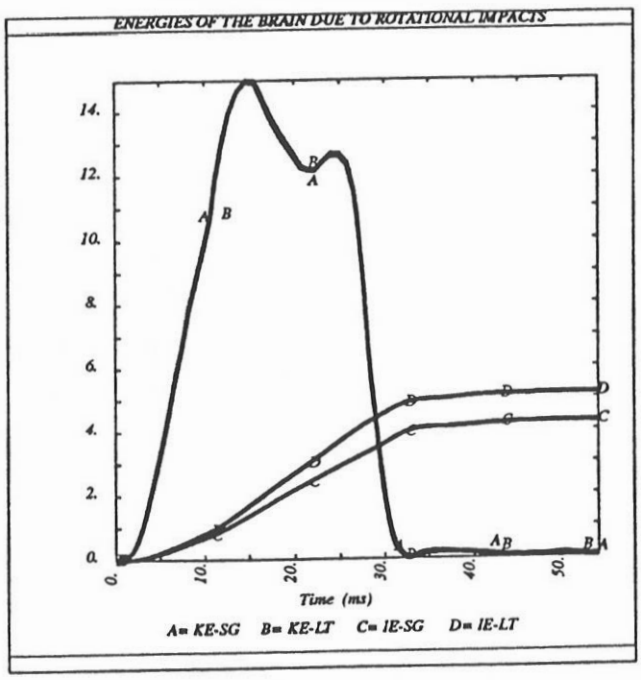

Fig. 6 Energies imparted to the brain due to rotations.

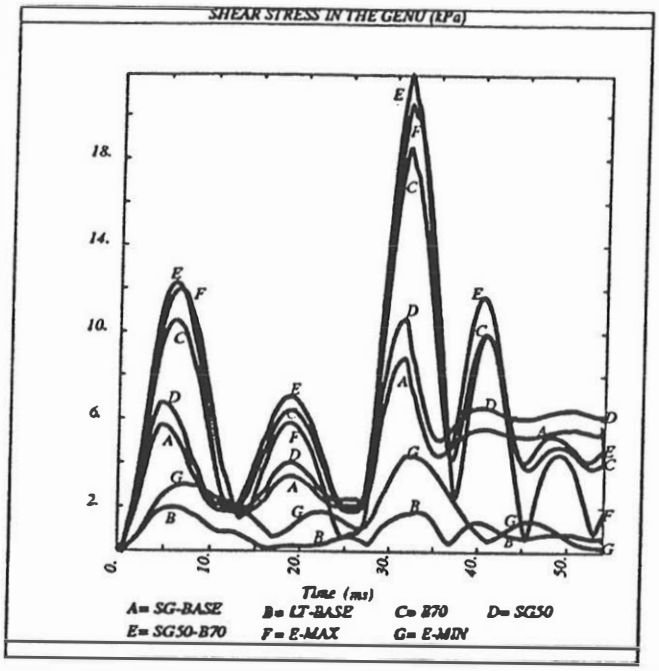

Fig. 7 Shear stresses in the genu due to rotations.

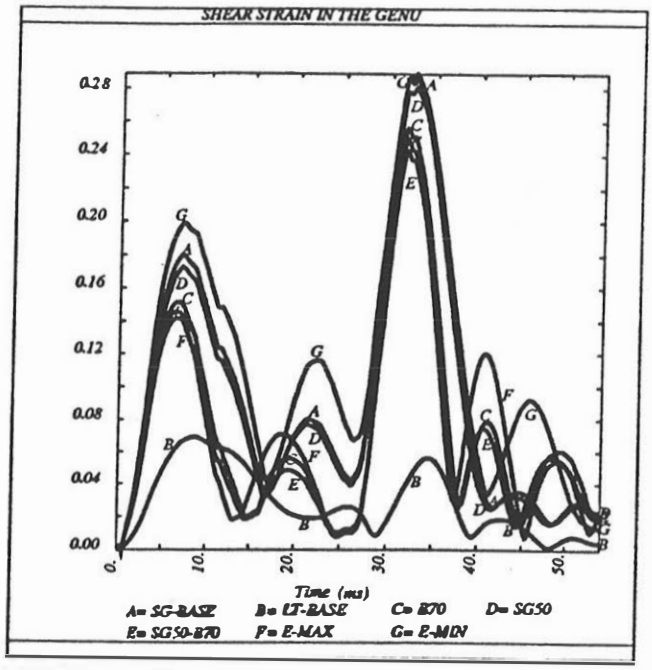

Fig. 8 Shear strains in the genu due to rotations.

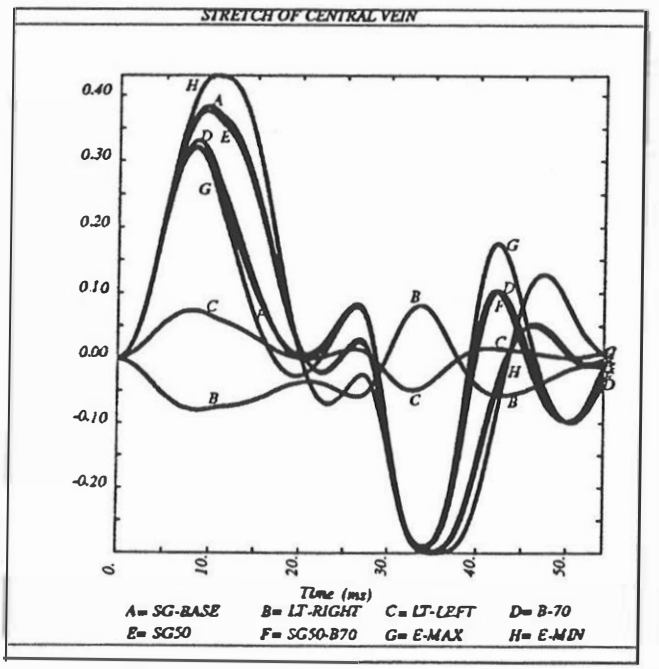

Fig. 9 Stretch of the central bridging veins due to rotations.

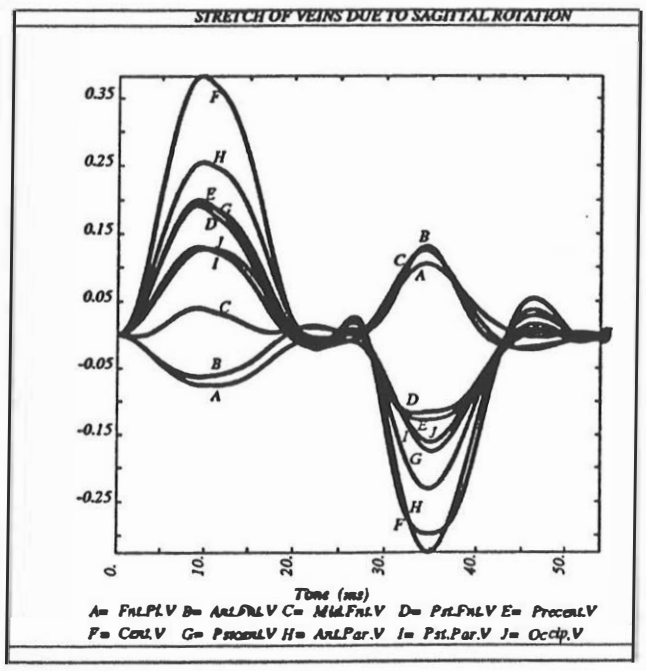

Fig. 10 Stretch of the bridging veins due to sagittal rotation.

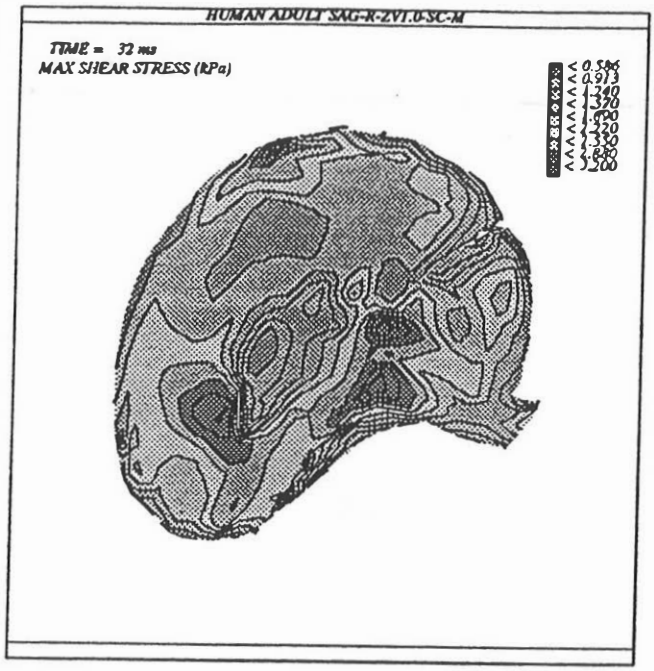

Fig. 11 Shear stress contours at 32 ms: sagittal rotation, parasagittal section.

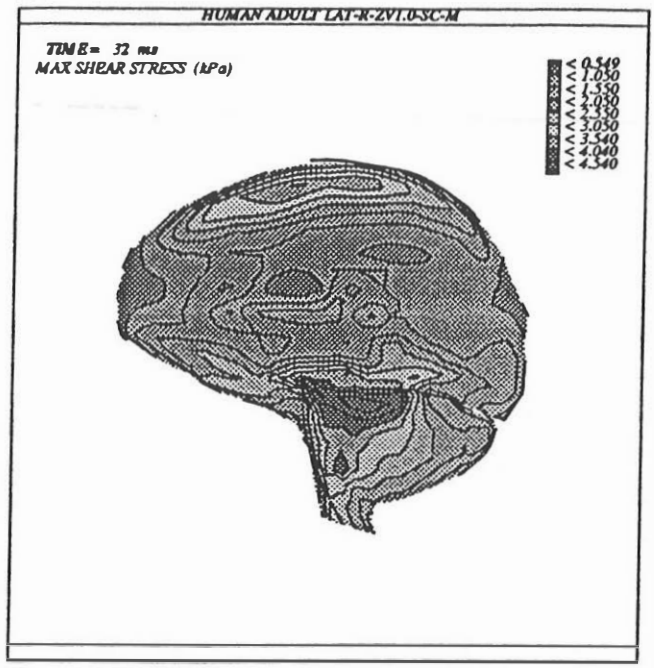

Fig. 12 Shear stress contours at 32 ms: lateral rotation, parasagittal section.

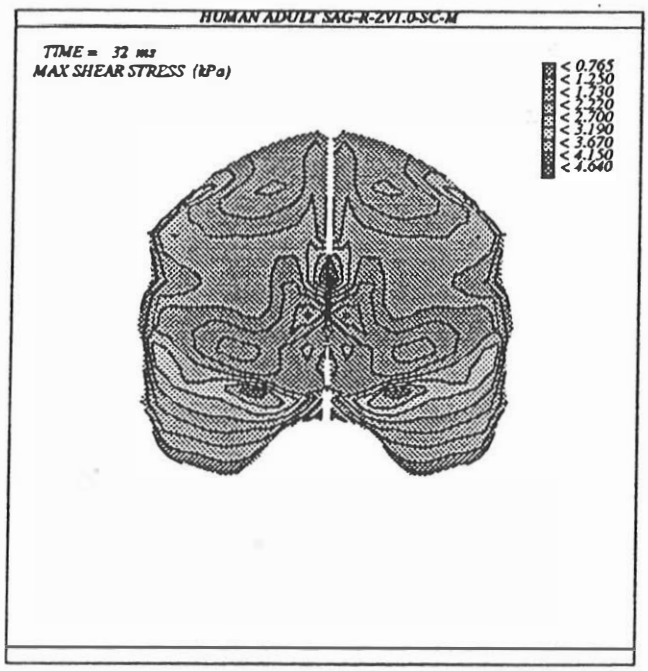

Fig. 13 Shear stress contours at 32 ms: sagittal rotation, coronal section in the forebrain.

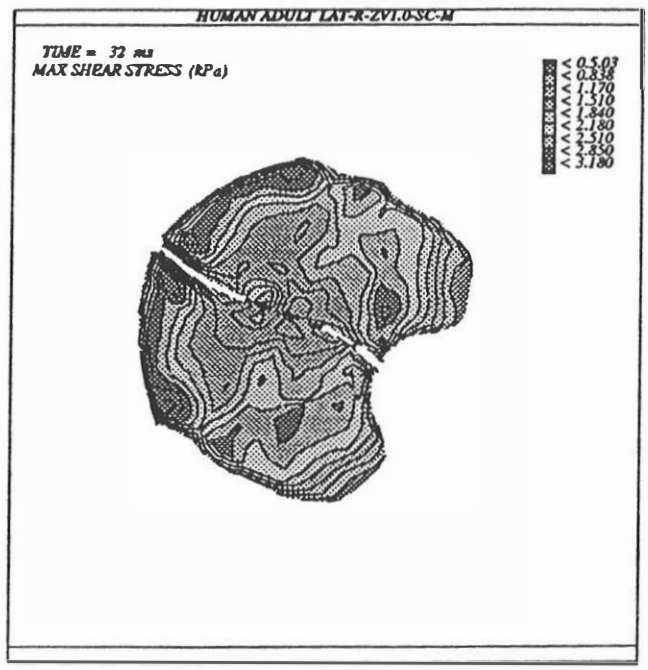

Fig. 14 Shear stress contours at 32 ms: lateral rotation, coronal section in the forebrain.

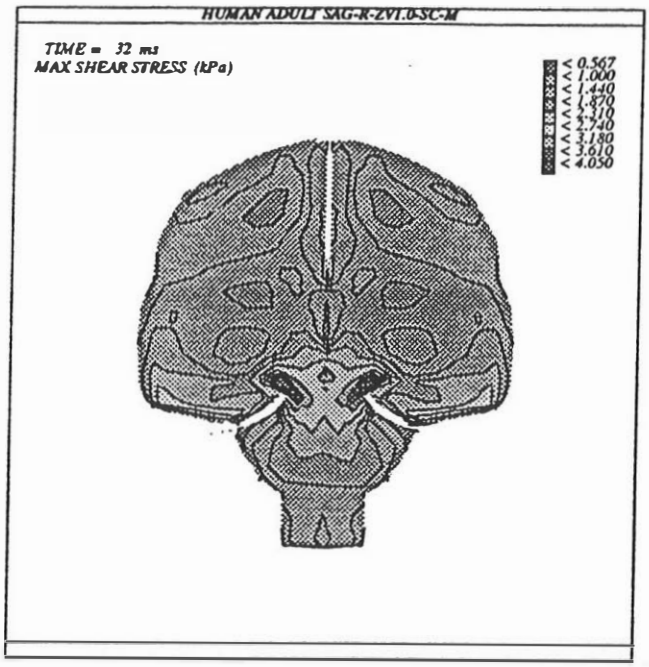

Fig. 15 Shear stress contours at 32 ms: sagittal rotation, coronal section in the midbrain.

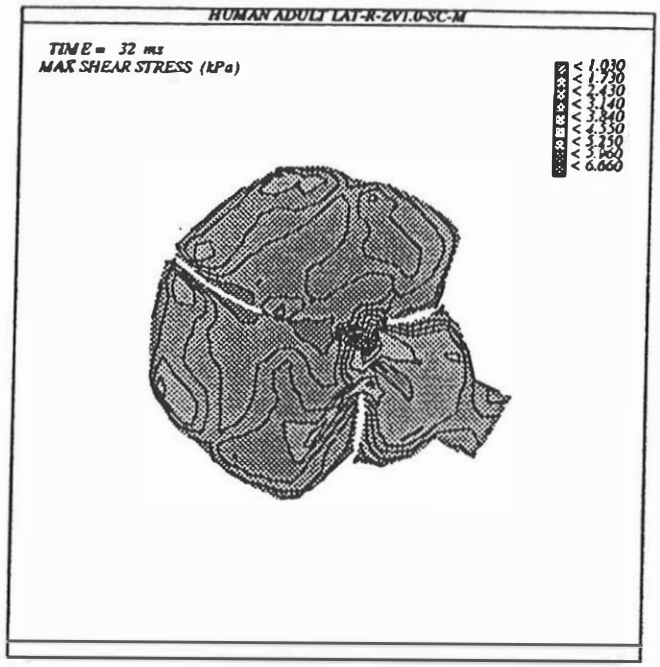

Fig. 16 Shear stress contours at 32 ms: lateral rotation, coronal section in the midbrain.